materials

MDPI

Article

Highly-Stable $Li_4Ti_5O_{12}$ Anodes Obtained by Atomic-Layer-Deposited Al_2O_3

Jae Kook Yoon [1], Seunghoon Nam [1], Hyung Cheoul Shim [1], Kunwoo Park [2], Taeho Yoon [2], Hyung Sang Park [2] and Seungmin Hyun [1,3,*]

[1] Nano Mechanical Systems Research Division, Department of Nano Mechanics, Korea Institute of Machinery and Materials (KIMM), Daejeon 34103, Korea; jkyoon@kimm.re.kr (J.K.Y.); kwek14@kimm.re.kr (S.N.); scafos@kimm.re.kr (H.C.S.)

[2] ISAC Research Inc., Daejeon 34036, Korea; kw.park@isacresearch.com (K.P.); th.yoon@isacresearch.com (T.Y.); hys.park@isacresearch.com (H.S.P.)

[3] Department of Nanomechatronics, University of Science and Technology (UST), Daejeon 34113, Korea

* Correspondence: hyun@kimm.re.kr; Tel.: +82-42-868-7981

Received: 18 April 2018; Accepted: 14 May 2018; Published: 16 May 2018



Abstract: LTO ($Li_4Ti_5O_{12}$) has been highlighted as anode material for next-generation lithium ion secondary batteries due to advantages such as a high rate capability, excellent cyclic performance, and safety. However, the generation of gases from undesired reactions between the electrode surface and the electrolyte has restricted the application of LTO as a negative electrode in Li-ion batteries in electric vehicles (EVs) and energy storage systems (ESS). As the generation of gases from LTO tends to be accelerated at high temperatures (40–60 °C), the thermal stability of LTO should be maintained during battery discharge, especially in EVs. To overcome these technical limitations, a thin layer of Al_2O_3 (~2 nm thickness) was deposited on the LTO electrode surface by atomic layer deposition (ALD), and an electrochemical charge-discharge cycle test was performed at 60 °C. The capacity retention after 500 cycles clearly shows that Al_2O_3-coated LTO outperforms the uncoated one, with a discharge capacity retention of ~98%. TEM and XPS analyses indicate that the surface reactions of Al_2O_3-coated LTO are suppressed, while uncoated LTO undergoes the (111) to (222) phase transformation, as previously reported in the literature.

Keywords: $Li_4Ti_5O_{12}$; atomic-layer-deposited Al_2O_3; gas evolution

1. Introduction

Lithium-ion batteries have been used as a power source for operating various small electronic devices, such as mobile phones and laptops. Moreover, mid- and large-size batteries are used in electronic vehicles (HEVs, PHEVs, and EVs) as well as in energy storage systems (ESS), which have recently been commercialized. Therefore, electrode materials with high capacity, high power, short charging times, and excellent lifetimes are essential for the performance and safety of the batteries meant for frequent use [1–5]. However, graphite and carbon-based materials, which are commercially used as negative electrodes, are now considered an impediment for fast-charging applications. One alternative to graphite is spinel $Li_4Ti_5O_{12}$ (LTO), which exhibits an excellent rate capability with superior cycle-life performance compared to existing anode material candidates. Moreover, as LTO has a relatively high reaction potential (1.55 V vs. Li/Li^+), an irreversible solid-electrolyte interphase (SEI) is not generated in the early stages of delithiation. Such advantageous characteristics highlight LTO as an appropriate material for electronic vehicles (HEVs, PHEVs, and EVs) and ESS [6–23].

One of the disadvantages of LTO is the degradation in the performance of the electrode caused by gas generation and electrolyte decomposition at the interface. As opposed to graphite and other

Li-alloy anodes, the absence of an irreversible SEI layer causes LTO to be in direct contact with the electrolyte and hence to be vulnerable to side reactions. Recent studies also showed that the transition-metal ions (Ti^{3+} and Ti^{4+}) present on the LTO surface violently react with the electrolyte, causing the electrolyte solvent to decompose during electrochemical cycling, thereby deteriorating the long-term stability of electrodes made of LTO. These reactions are particularly accelerated in high-temperature environments, which has adverse effects on the cyclability of the electrode [24–26]. For LTO to be employed in EV and ESS applications as fast-chargeable anodes, the safety of the LTO material under high-temperature conditions must be ensured; otherwise the accelerated side reactions could result in unexpected explosive accidents. The stability of LTO electrodes has been enhanced by using carbon-based materials to separate LTO from the surrounding electrolyte, resulting in visibly reduced side reactions [27,28]. However, these approaches were not quite effective to suppress gas evolution during electrode cycling, especially at elevated temperatures. Considering that EVs tend to run in the daytime, the electrochemical performances of LTO electrodes should be guaranteed even under certain extreme circumstances.

Herein, aluminum oxide (Al_2O_3) was directly deposited on an LTO electrode by atomic layer deposition (ALD), and its cycle-life performance was evaluated at 60 °C to identify an effective way to prevent gas evolution in LTO. The formation of an ultra-thin Al_2O_3 layer (~2 nm thickness) on an electrode does not significantly affect the electrical conductivity, and therefore, 98% of the theoretical capacity of LTO is retained even after 500 cycles at 60 °C. LTO without an Al_2O_3 layer degrades upon cycling, and it is clearly seen that pouch-type cells made of uncoated LTO inflate as a result of gas generation (CO, CO_2, H_2, etc.). The role of the Al_2O_3 layer was verified by transmission electron microscopy (TEM) and X-ray photoelectron spectroscopy (XPS). Neither a distortion of the LTO (111) plane nor a change in the oxidation state of Ti was detected on the Al_2O_3-coated LTO, whereas a change in the interfacial phase of the uncoated LTO and shifts in the oxidation state (Ti^{3+}) were observed after cycling.

2. Experimental

2.1. Preparation of the LTO Powder and Al_2O_3-Coated LTO Electrode

To synthesize LTO powder, Li_2CO_3 and TiO_2 were mixed at a molar ratio of 4.2:5 in acetone and dried at room temperature for approximately one hour to form a Li_2CO_3/TiO_2 mixture. The Li_2CO_3/TiO_2 mixture was heat-treated in a tube furnace in an Ar/H_2 atmosphere at 850 °C for 10 h, and the resulting powder was further ground to obtain LTO powder [29]. The prepared LTO was uniformly mixed with carbon black and PVDF at a mass ratio of 80:10:10 in *N*-methyle-2-pyrroledine (NMP) to prepare an electrode slurry. The LTO electrode active material slurry was coated to a thickness of ~20 μm onto a Cu foil using a doctor blade, and further vacuum-dried at 110 °C to fabricate a LTO electrode. An Al_2O_3-protective layer was deposited with a thickness of several nanometers on the fabricated LTO electrode by ALD. ALD is the most effective approach compared to other deposition methods (such as sol-gel and CVD), since it allows one to adjust the thickness in Å units and uniformly deposit a protective layer [30–34].

2.2. Physical Characterization

X-ray diffraction analysis (XRD, Empyrean PAN analytical, Almelo, The Netherlands) was conducted in the range of $2\theta = 10°–70°$ with Cu K α radiation for structural analysis of the synthesized LTO powder. The shape, particle size, and surface changes were observed by field emission-scanning electron microscopy (FE-SEM, JSM-7800F, JEOL, Tokyo, Japan) and transmission electron microscopy (TEM, Tecnai F20 G^2 Microscope (FEI, Hillsboro, OR, USA) operated at 200 kV). The oxidation state of Ti was investigated by X-ray photoelectron spectroscopy (XPS, AXIS-HIS: KRATOS, Manchester, UK) with incident photon of 1254 eV.

2.3. Electrochemical Tests

A pouch-type LTO half-cell was fabricated to analyze the electrochemical characteristics of the materials. The uncoated and Al_2O_3-coated LTO were used as the working electrode with an area of 4 cm^2, and lithium metal was used as the counter electrode. An olefin-based membrane (Celgard 2400, Celgard Inc., Charlotte, NC, USA) was used as a separator. The membrane was inserted into an Al pouch, a 1 M $LiPF_6$ electrolyte in a solution of ethylene carbonate (EC) and diethyl carbonate (DEC) (soulbrain, Seongnam, Korea) at a 1:1 volume ratio was also introduced, and the pouch was vacuum-sealed. The electrochemical charge-discharge behaviors and the cycle life performance of the fabricated LTO pouch cell were studied using a galvanostatic charge/discharge cycler (WBCS3000, Wonatech, Seoul, Korea) at 60 °C in a constant-temperature chamber. The voltage range was set between 0.9 V and 2.6 V. The value of 1 C was considered based upon the theoretical capacity of LTO (175 mAh/g). Electrochemical impedance spectroscopy (EIS) of the electrode was conducted using an electrochemical workstation (ZIVE MP1, Wonatech, Seoul, Korea) in a frequency range of 10^5–10^{-1} Hz.

3. Results and Discussion

3.1. Synthesis of LTO

Figure 1 shows the XRD pattern of the synthesized LTO powder. The diffraction peaks are indexed to the standard diffraction peaks of spinel LTO (JCDPS No. 49-0207). The synthesized LTO powder reveals the spinel structure with little amount of TiO_2 (rutile) impurities. L. J. Wan et al., claimed that such a small fraction of rutile TiO_2 at the surface of LTO is beneficial for its rate capability [35]. Furthermore, the shape of the synthesized LTO powder was observed by SEM. As shown in Figure 2, the images clearly display aggregated forms of the LTO, composed of spherical primary particles of several hundreds of nanometers to several micrometers in diameter. The hierarchy of the particles are advantageous for the Li-ion diffusion due to short diffusion path through the nanometer-sized primary particles and high accessibility of electrolyte to the active electrode material owing to the porous structure. The aggregated form of LTO is also beneficial for achieving high tap density of electrodes.

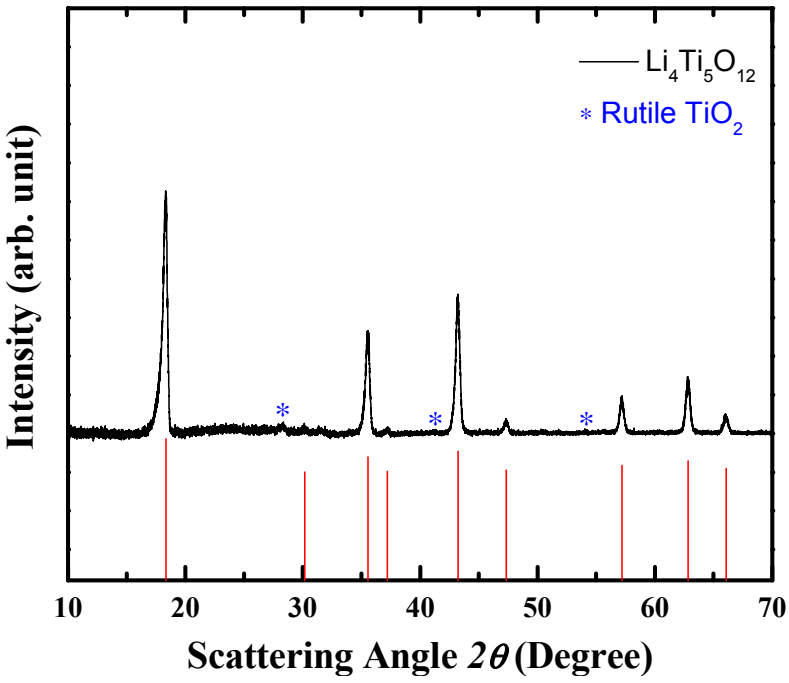


Figure 1. XRD patterns of LTO ($Li_4Ti_5O_{12}$) powder. The ideal peak positions and intensities for LTO (JCPDS No. 49-0207) are marked at the bottom. Possible TiO_2 impurities are denoted by stars.

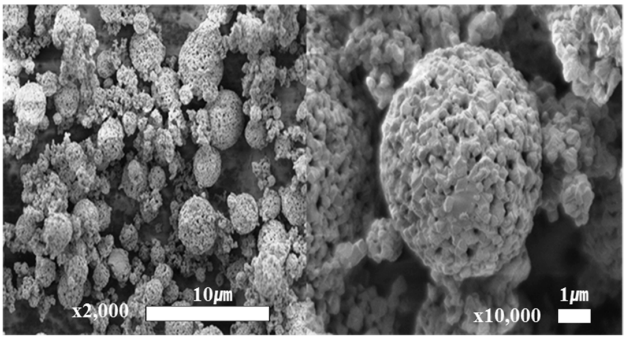


Figure 2. SEM images of synthesized LTO powder.

3.2. Schematic Diagram and Morphology of Uncoated and Al_2O_3-Coated LTO Electrodes

Figure 3 illustrates the process and effect of the Al_2O_3 coating on the electrochemical performance of LTO. As shown in Figure 3a, the electrode was initially constructed with LTO as an active material prior to Al_2O_3 coating. During the electrochemical charge/discharge cycles at a temperature of 60 °C, the uncoated LTO electrode surface was directly exposed to the electrolyte, resulting in several side reactions, as a result of which leads to gas (CO, CO_2, and O_2) evolution as well as a phase transformation of the crystalline LTO. However, when a thin and conformal Al_2O_3 layer was deposited on the LTO electrode by ALD, direct contact with the electrolyte was prevented, resulting in negligible side reactions between the electrolyte and the electrode surface. Thus, the initial state of the LTO electrode was maintained without any damage or phase transformation during the high-temperature electrochemical charge/discharge cycles. The effect of Al_2O_3 coating is more notable by a focused-ion beam (FIB) image (Figure S1) after charge-discharge at 60 °C, as shown in Figure 3b. It can also be observed by TEM images that the surface of the LTO electrode was coated by a thin Al_2O_3 protective layer. Figure 4a shows the (111) plane of the uncoated LTO electrode surface, confirming that the surface has a typical spinel structure. From Figure 4b,c, it is seen that an Al_2O_3 layer is uniformly formed on the surface of the LTO electrode with a thickness of ~2.5 nm. The formation of the protective layer on the electrode surface was carefully confirmed by EDS mapping.

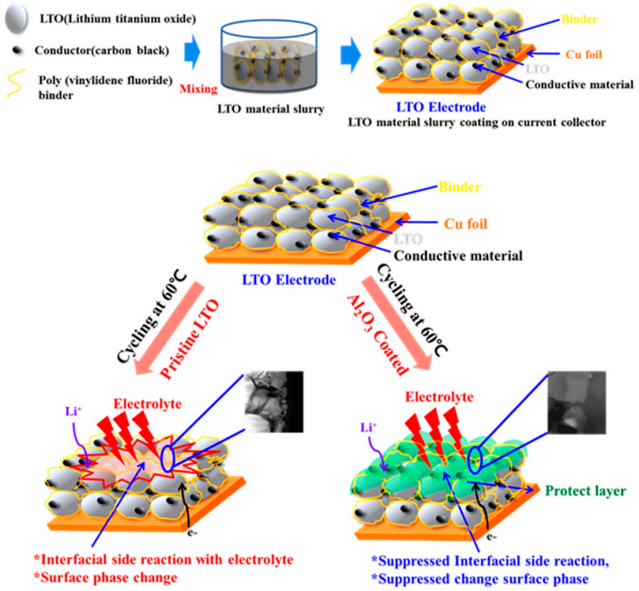


Figure 3. Schematic diagram of (**a**) fabrication of LTO electrode and (**b**) expected phenomena of uncoated and Al_2O_3-coated LTO electrode cycled at 60 °C.

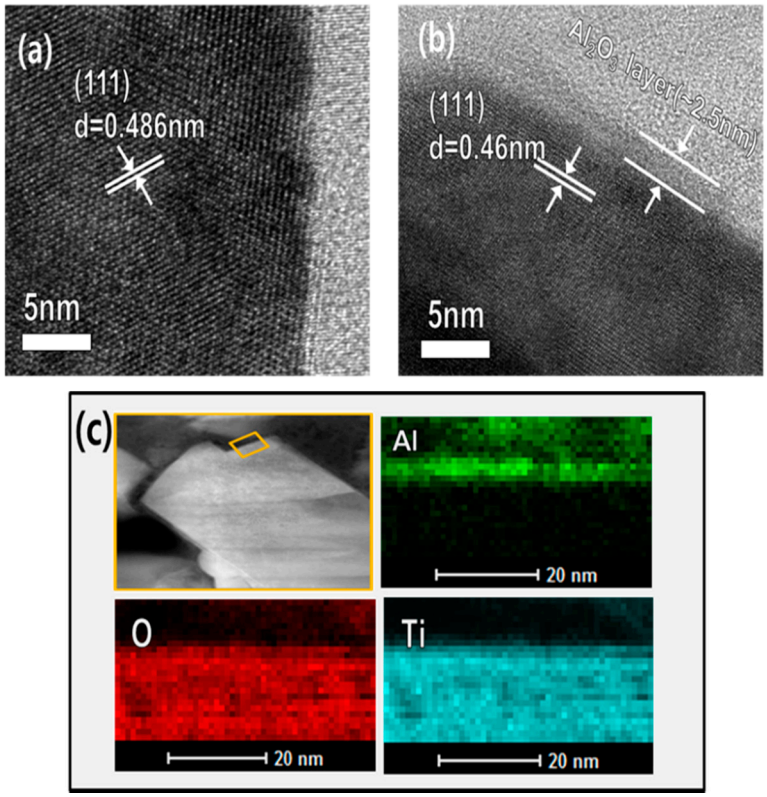


Figure 4. HRTEM Images of the (**a**) uncoated and (**b**) Al_2O_3-coated LTO electrode at the pristine state. (**c**) EDX elemental mapping of the Al_2O_3-coated LTO electrode.

3.3. Electrochemical Properties of the Uncoated and Al_2O_3-Coated LTO after Cycles at a 60 °C

Pouch cells (half cells) were assembled using the uncoated and Al_2O_3-coated LTO electrodes to identify and compare the electrochemical charge-discharge behavior and cyclability. For the uncoated one, a relatively significant reduction in capacity with respect to the initial capacity (from 161 mAh/g to 128 mAh/g) was observed after 500 electrochemical charge/discharge cycles at high temperature (60 °C), which demonstrates more unstable behavior (~79% capacity retention), compared to that at room temperature (Figure S2). This observation indicates that the characteristics of the LTO electrode do not change significantly during the electrochemical charge/discharge cycles at room temperature. However, as mentioned in the Introduction, side reactions with the electrolyte are accelerated at high temperatures, which could lead to a reduction in electrochemical stability. To address this problem, the surface of the LTO electrode was coated with Al_2O_3, and Figure 5 shows the evaluation and comparison of the characteristics of the Al_2O_3-coated LTO. The Al_2O_3-coated LTO electrode (Figure 5a) exhibits a remarkably stable charge/discharge behavior as well as minimal reduction in capacity with respect to the initial capacity (from 164 mAh/g to 161 mAh/g) (Figure 5b) with the capacity retained up to ~98% of the initial one. As shown in Figure 5c, the capacity change of Al_2O_3-coated LTO during cycles exhibits a behavior that is clearly different than that of the uncoated LTO at high temperature (60 °C). Obviously, the Al_2O_3 on the LTO electrode surface separates the electrode surface from the electrolyte during the electrochemical charge/discharge cycles. Moreover, the coated Al_2O_3 acts as a protective layer that prevents electrolyte decomposition caused by side reactions between the electrolyte and electrode surface, especially at high temperatures. The Al_2O_3 coating improves the electrochemical cycle performance and stability. Meanwhile, the formation of ultra-thin Al_2O_3 layer (~2 nm thickness) on LTO electrodes does not significantly affect the electrical conductivity and battery performance, as confirmed by EIS (Figure S3), charge/discharge capacities at various C rates (Figure S4), and cycle-life performance with various thickness of Al_2O_3 (Figure S5).

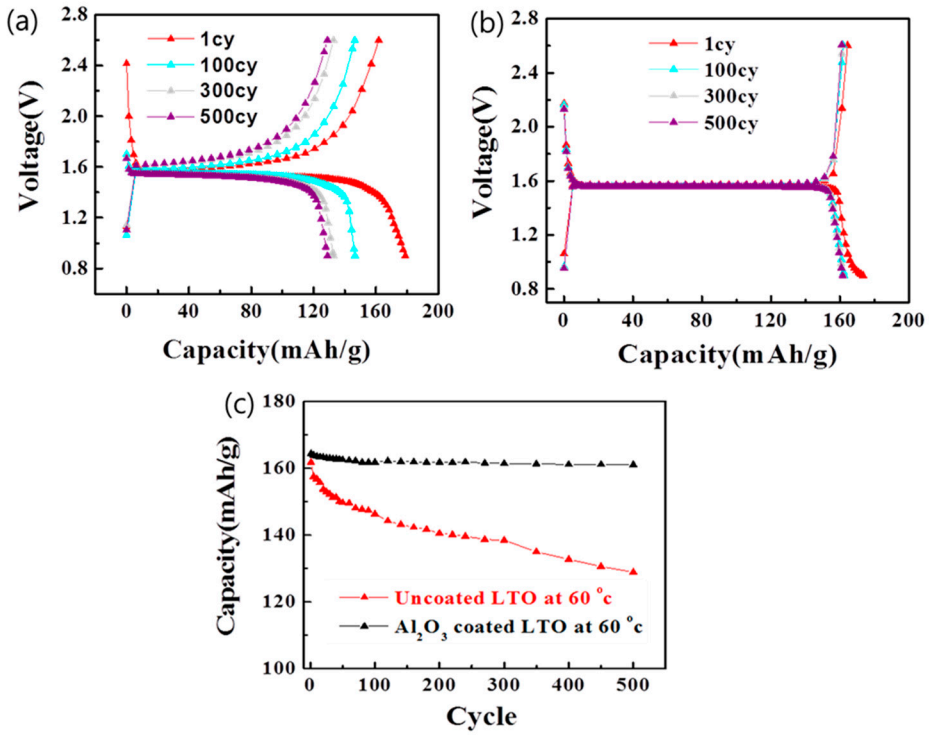


Figure 5. Voltage profiles of the (**a**) Al_2O_3-coated and (**b**) uncoated LTO at 60 °C. (**c**) Cycle-life performances of Al_2O_3-coated and uncoated LTO at 60 °C. The cells are discharged and charged within a voltage range of 2.6 and 0.9 V at 2 C (2 C = 250 mA/g based upon the theoretical capacity of LTO: 175 mAh/g).

Figure 6 shows the morphological changes in the uncoated and Al_2O_3-coated LTO after electrochemical charge/discharge at high temperature (60 °C). As shown in Figure 6a, the (222) phase plane, which is different from the (111) phase plane with a typical spinel structure, was identified on the outermost layer of the uncoated LTO electrode surface. At the high temperature of 60 °C, charging the uncoated LTO electrode accelerates the side reaction between the Ti^{3+} ions remaining on the electrode surface and the electrolyte solvent, which results in the decomposition of the electrolyte and the generation of gases. Furthermore, this side reaction depletes O_2^{2-} ions from the outermost electrode, leading to partial phase change of LTO crystals, as seen in Figure 6a. The side reaction is reflected as a reduction in the electrochemical capacity upon cycling, which would be more serious in applications for large-sized batteries [24,29]. However, the Al_2O_3-coated LTO exhibited no sign of phase change on the surface of the electrode, maintaining the (111) phase plane with a spinel structure even after 500 cycles at 60 °C (Figure 6b). The Ti 2*p* X-ray photoelectron spectra (XPS) of the uncoated and Al_2O_3-coated LTO electrodes (Figure 7) show that Ti 2*p* spectrum of the uncoated LTO shifts to lower binding energy compared to the pristine and Al_2O_3-coated LTO, indicating that depleted O^{2-} ions accompanies the permanent change of Ti oxidation state, which, otherwise, should have turned back to nearly Ti^{4+} state when the electrode is charged. The FIB images also corroborate that the Al_2O_3-coated LTO electrode maintained a stable state without damages or changes on the electrode level, compared to that of the uncoated LTO (Figure S1).

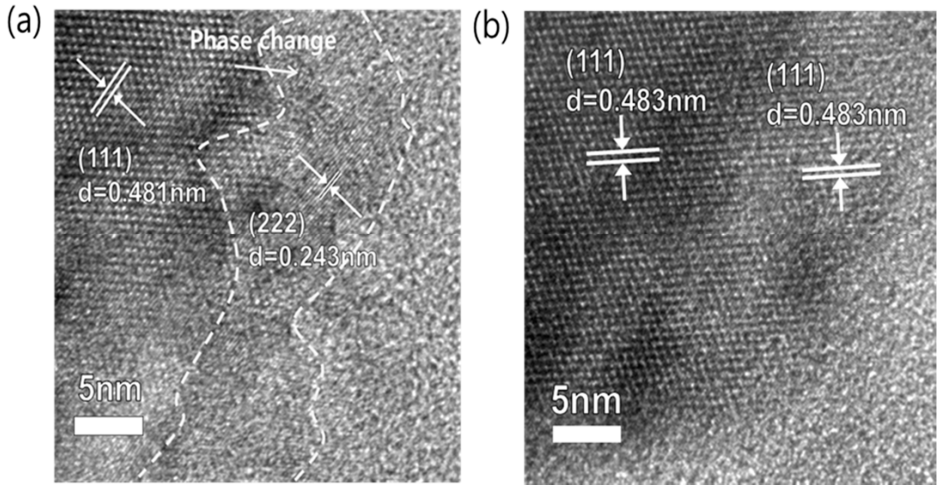


Figure 6. HRTEM images of the (**a**) uncoated and (**b**) Al_2O_3-coated LTO electrode after 500 cycles at 60 °C. The electrodes are in a charged state.

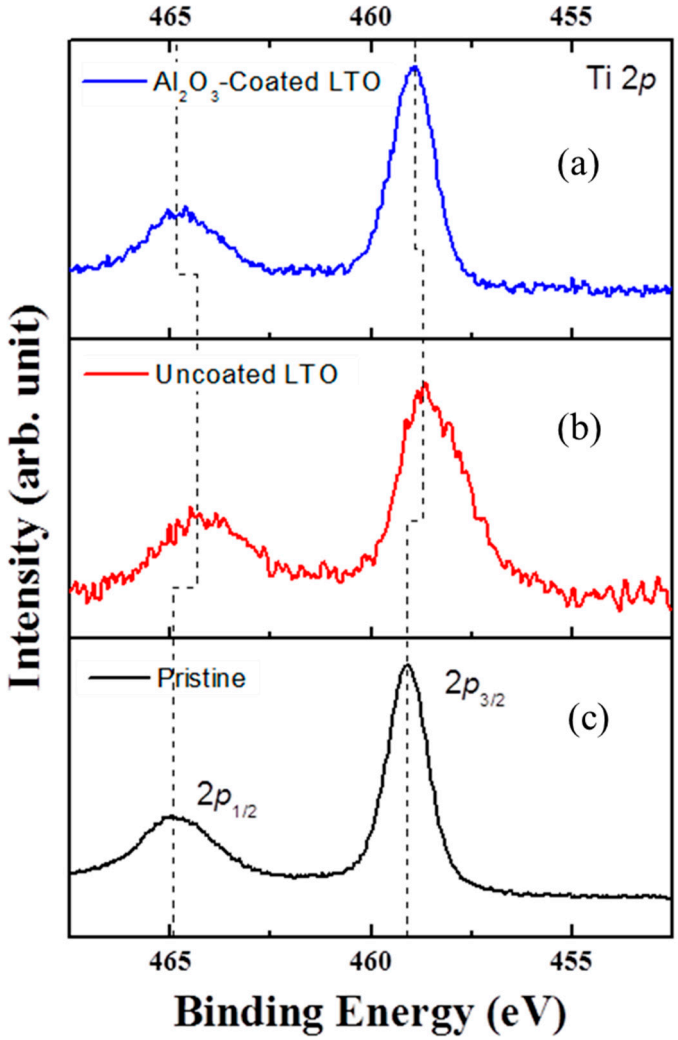


Figure 7. Ti 2*p* X-ray photoelectron spectra (XPS) of the LTO electrodes. (**a**) Pristine state, and charged states of the (**b**) uncoated and (**c**) Al_2O_3-coated LTO electrode after 500 cycles. The dashed lines are drawn to guide eyes.

4. Conclusions

In order to improve the high-temperature stability of the LTO ($Li_4Ti_5O_{12}$) anode, an ultra-thin and uniform Al_2O_3 protective layer (~2 nm thickness) was directly coated on the electrode surface using ALD. The Al_2O_3-coated LTO electrode showed an excellent electrochemical cycle-life performance, retaining 98% of the initial capacity after 500 cycles. The outermost (111) plane of the coated LTO was maintained without any damage nor phase transformation, compared to the uncoated LTO electrode. Al_2O_3 acted as a protective layer that suppressed side reactions at the interface between the LTO electrode and electrolyte, which could have been accelerated at high temperature. Accordingly, the formation of an ultra-thin and uniform Al_2O_3 protective layer onto the LTO electrode surface is an effective method to improve the high-temperature stability of LTO electrodes.

Supplementary Materials: The following are available online at http://www.mdpi.com/1996-1944/11/5/803/s1, Figure S1: FIB images the (**a**) uncoated and (**b**) Al_2O_3-coated LTO after 500 cycle at 60 °C. The electrode are in a charged state. Figure S2: Charge and discharge curves of uncoated LTO (**a**) at 25 °C, (**b**) at 60 °C, (**c**) Cycle-life performances of the uncoated LTO cycled at 25 °C and 60 °C. The cells are discharged and charged within a voltage range of 2.6 and 0.9 V at 2 C. (2C = 250 mA/g based upon the theoretical capacity of LTO: 175 mAh/g). Figure S3: Nyquist plots of the uncoated and Al_2O_3-coated LTO electrodes. Figure S4: Galvanostatic charge-discharge tests of the uncoated and Al_2O_3-coated LTO electrode at different current densities varied from 0.1 to 20 C. Figure S5: Comparison of the Al_2O_3-coated LTO electrodes having different thicknesses.

Author Contributions: Conceptualization, J.K.Y. and S.N.; Methodology, H.C.S., K.P., T.Y. and H.S.P.; Validation, J.K.Y., S.N. and S.H.; Formal Analysis, J.K.Y., S.N. and S.H.; Writing-Original Draft Preparation, J.K.Y. and S.N.; Writing-Review & Editing, S.H.

Funding: This research was funded by the Korea Institute of Machinery and Materials (NK211B) and the National Research Council of Science & Technology (NST) grant by the Korea government (No. CAP-13-01-KITECH).

Acknowledgments: This work was supported by the Korea Institute of Machinery and Materials (KIMM) funding (NK211B) and the National Research Council of Science & Technology (NST) grant by the Korea government (No. CAP-13-01-KITECH). The authors would also like to thank Cheol-Hwee Shim and Jae-Pyoung Ahn in ACC (Advanced Analysis Center) of KIST (Korea Insititute of Science and Technology) for their help with the TEM analyses.

Conflicts of Interest: The authors declare no conflict of interest.

References

1. Belharouak, I.; Koenig, G.M., Jr.; Amine, K. Electrochemistry and safety of $Li_4Ti_5O_{12}$ and graphite anodes paired with $LiMn_2O_4$ for hybrid electric vehicle Li-ion battery applications. *J. Power Sources* **2011**, *196*, 10344–10350. [CrossRef]
2. Tarascon, J.-M.; Armand, M. Issues and challenges facing rechargeable lithium batteries. *Nature* **2001**, *414*, 359–367. [CrossRef] [PubMed]
3. Bruce, P.G.; Scrosati, B.; Tarascon, J.-M. Nanomaterials for rechargeable lithium batteries. *Angew. Chem. Int. Ed.* **2008**, *47*, 2930–2946. [CrossRef] [PubMed]
4. Belharouak, I.; Amine, K. $Li_2MTi_6O_{14}$ (M = Sr, Ba): New anodes for lithium-ion batteries. *Electrochem. Commun.* **2003**, *5*, 435–438. [CrossRef]
5. Goodenough, J.B.; Kim, Y. Challenges for rechargeable Li batteries. *Chem. Mater.* **2010**, *22*, 587–603. [CrossRef]
6. Sun, X.; Radovanovic, P.V.; Cui, B. Advances in spinel $Li_4Ti_5O_{12}$ anode materials for lithium-ion batteries. *New J. Chem.* **2015**, *39*, 38–63. [CrossRef]
7. Wu, F.; Wang, Z.; Li, X.; Guo, H. Synthesis of high performance $Li_4Ti_5O_{12}$ microspheres and TiO_2 nanowires from natural ilmenite. *RSC Adv.* **2014**, *4*, 40111–40119. [CrossRef]
8. Aricò, A.S.; Bruce, P.; Scrosati, B.; Tarascon, J.-M.; Schalkwijk, W.V. Nanostructured materials for advanced energy conversion and storage devices. *Nat. Mater.* **2005**, *4*, 366–377. [CrossRef] [PubMed]
9. Takami, N.; Inagaki, H.; Kishi, T.; Harada, Y.; Fujita, Y.; Hoshina, K. Electrochemical kinetics and safety of 2-volt class Li-ion battery system using lithium titanium oxide anode. *J. Electrochem. Soc.* **2009**, *156*, A128–A132. [CrossRef]
10. Zaghib, K.; Simoneau, M.; Armand, M.; Gauthier, M. Electrochemical study of $Li_4Ti_5O_{12}$ as negative electrode for Li-ion polymer rechargeable batteries. *J. Power Sources* **1999**, *81*, 300–305. [CrossRef]

11. Wagemaker, M.; van Eck, E.R.H.; Kentgens, A.P.; Mulder, F.M. Li-Ion Diffusion in the Equilibrium Nanomorphology of Spinel $Li_{4+x}Ti_5O_{12}$. *J. Phys. Chem. B* **2009**, *113*, 224–230. [CrossRef] [PubMed]
12. Yang, X.; Huang, Y.; Wang, X.; Jia, D.; Pang, W.K.; Guo, Z.; Tang, X. High rate capability core–shell lithium titanate@ ceria nanosphere anode material synthesized by one-pot co-precipitation for lithium-ion batteries. *J. Power Sources* **2014**, *257*, 280–285. [CrossRef]
13. Lin, C.; Fan, X.; Xin, Y.; Cheng, F.; Lai, M.O.; Zhou, H.; Lu, L. $Li_4Ti_5O_{12}$-based anode materials with low working potentials, high rate capabilities and high cyclability for high-power lithium-ion batteries: A synergistic effect of doping, incorporating a conductive phase and reducing the particle size. *J. Mater. Chem. A* **2014**, *2*, 9982–9993. [CrossRef]
14. Ouyang, C.Y.; Zhong, Z.Y.; Lei, M.S. Ab initio studies of structural and electronic properties of $Li_4Ti_5O_{12}$ spinel. *Electrochem. Commun.* **2007**, *9*, 1107–1112. [CrossRef]
15. Yin, Y.H.; Li, S.Y.; Fan, Z.J.; Ding, X.L.; Yang, S.T. Synthesis of novel anode $Li_4Ti_5O_{12}$/C with PAN as carbon source and its electrochemical performance. *Mater. Chem. Phys.* **2011**, *130*, 186–190. [CrossRef]
16. Wang, G.J.; Gao, J.; Fu, L.J.; Zhao, N.H.; Wu, Y.P.; Takamura, T. Preparation and characteristic of carbon-coated $Li_4Ti_5O_{12}$ anode material. *J. Power Sources* **2007**, *174*, 1109–1112. [CrossRef]
17. Huang, S.H.; Wen, Z.Y.; Zhu, X.J.; Yang, X.L. Research on $Li_4Ti_5O_{12}$/CuxO Composite Anode Materials for Lithium-Ion Batteries. *J. Electrochem. Soc.* **2005**, *152*, A1301–A1305. [CrossRef]
18. Oh, Y.; Nam, S.; Wi, S.; Kang, J.H.; Hwang, T.H.; Lee, S.H.; Park, H.H.; Cabana, J.; Kim, C.; Park, B. Effective wrapping of graphene on individual $Li_4Ti_5O_{12}$ grains for high-rate Li-ion batteries. *J. Mater. Chem. A* **2014**, *2*, 2023–2027. [CrossRef]
19. Liu, J.; Li, X.F.; Cai, M.; Li, R.; Sun, X.L. Ultrathin atomic layer deposited ZrO_2 coating to enhance the electrochemical performance of $Li_4Ti_5O_{12}$ as an anode material. *Electrochim. Acta* **2013**, *93*, 195–201. [CrossRef]
20. Snyder, M.Q.; Trebukhova, S.A.; Ravdel, B.; Wheeler, M.C.; Carlo, J.D.; Tripp, C.P.; DeSisto, W.J. Synthesis and characterization of atomic layer deposited titanium nitride thin films on lithium titanate spinel powder as a lithium-ion battery anode. *J. Power Sources* **2007**, *165*, 379–385. [CrossRef]
21. Kim, J.; Lee, K.E.; Kim, K.H.; Wi, S.; Lee, S.; Nam, S.; Kim, C.; Kim, S.O.; Park, B. Single-layer graphene-wrapped $Li_4Ti_5O_{12}$ anode with superior lithium storage capability. *Carbon* **2017**, *114*, 275–283. [CrossRef]
22. Liu, J.; Bian, P.; Li, J.; Ji, W.; Hao, H.; Yu, A. Gassing behavior of lithium titanate based lithium ion batteries with different types of electrolytes. *J. Power Sources* **2015**, *286*, 380–387. [CrossRef]
23. Belharouak, I.; Koening, G.M., Jr.; Tan, T.; Yumoto, H.; Ota, N.; Amine, K. Performance degradation and gassing of $Li_4Ti_5O_{12}$/$LiMn_2O_4$ lithium-ion cells. *J. Electrochem. Soc.* **2012**, *159*, A1165–A1170. [CrossRef]
24. Amine, K.; Belharouak, I.; Chen, Z.; Tran, T.; Yumoto, H.; Ota, N.; Myung, S.T.; Sun, Y.K. Nanostructured anode material for high-power battery system in electric vehicles. *Adv. Mater.* **2010**, *22*, 3052–3057. [CrossRef] [PubMed]
25. He, M.L.; Castel, E.; Laumann, A.; Nuspl, G.; Novák, P.; Berga, E.J. In situ gas analysis of $Li_4Ti_5O_{12}$ based electrodes at elevated temperatures. *J. Electrochem. Soc.* **2015**, *162*, A870–A876. [CrossRef]
26. Wu, K.; Yang, J.; Zhang, Y.; Wang, C.; Wang, D. Investigation on $Li_4Ti_5O_{12}$ batteries developed for hybrid electric vehicle. *J. Appl. Electrochem.* **2012**, *42*, 989–995. [CrossRef]
27. He, Y.B.; Li, B.; Liu, M.; Zhang, C.; Lv, W.; Yang, C.; Li, J.; Du, H.; Zhang, B.; Yang, Q.H.; Kim, J.K.; Kang, F. Gassing in $Li_4Ti_5O_{12}$-based batteries and its remedy. *Sci. Rep.* **2012**, *2*, 913. [CrossRef] [PubMed]
28. Li, X.; Xu, J.; Hwang, P.; Yang, W.; Wang, Z.; Wang, M.; Huang, Y.; Zhou, Y.; Qu, M.; Yu, Z.; Lin, Y. In-situ carbon coating to enhance the rate capability of the $Li_4Ti_5O_{12}$ anode material and suppress the electrolyte reduction decomposition on the electrode. *Electrochim. Acta* **2016**, *190*, 69–75. [CrossRef]
29. Xiao, L.J.; Higgins, X.; Lee, D.C.; Hassan, F.; Chen, Z.W. Hierarchical $Li_4Ti_5O_{12}$-TiO_2 composite microsphere consisting of nanocrystals for high power Li-ion batteries. *Electrochim. Acta* **2013**, *108*, 104–111.
30. Schwartzberg, A.M.; Olynick, D. Complex materials by atomic layer deposition. *Adv. Mater.* **2015**, *27*, 5778–5784. [CrossRef] [PubMed]
31. Marichy, C.; Bechelany, M.; Pinna, N. Atomic layer deposition of nanostructured materials for energy and environmental applications. *Adv. Mater.* **2012**, *24*, 1017–1032. [CrossRef] [PubMed]

32. Park, J.H.; Seo, J.; Park, S.; Shin, S.S.; Kim, Y.C.; Jeon, N.J.; Shin, H.-W.; Ahn, T.K.; Noh, J.H.; Yoon, S.C.; Hwang, C.S.; Seok, S.I. Efficient $CH_3NH_3PbI_3$ Perovskite Solar Cells Employing Nanostructured p-Type NiO Electrode Formed by a Pulsed Laser Deposition. *Adv. Electron. Mater.* **2015**, *27*, 4013–4019. [CrossRef] [PubMed]
33. George, S.M. Atomic layer deposition: An overview. *Chem. Rev.* **2010**, *110*, 111–131. [CrossRef] [PubMed]
34. Kim, H.; RamLee, H.B.; Maeng, W.J. Applications of atomic layer deposition to nanofabrication and emerging nanodevices. *Thin Solid Films* **2009**, *517*, 2563–2580. [CrossRef]
35. Wang, Y.-Q.; Gu, L.; Guo, Y.-G.; Li, H.; He, X.-Q.; Tsukimoto, S.; Ikuhara, Y.; Wan, L.J. Rutile-TiO_2 nanocoating for a high-rate $Li_4Ti_5O_{12}$ anode of a lithium-ion battery. *J. Am. Chem. Soc.* **2012**, *134*, 7874–7879. [CrossRef] [PubMed]



© 2018 by the authors. Licensee MDPI, Basel, Switzerland. This article is an open access article distributed under the terms and conditions of the Creative Commons Attribution (CC BY) license (http://creativecommons.org/licenses/by/4.0/).